Analyst

RSC Publishing

PAPER

View Article Online
View Journal

Cite this: DOI: 10.1039/c3an00190c

A rapid electrochemical biosensor based on an AC electrokinetics enhanced immuno-reaction†

I-Fang Cheng,[a] Hsiao-Lan Yang,[b] Cheng-Che Chung[c] and Hsien-Chang Chang*[bde]

Received 25th January 2013
Accepted 13th May 2013

DOI: 10.1039/c3an00190c

www.rsc.org/analyst

Fluorescent labelling and chromogenic reactions that are commonly used in conventional immunoassays typically utilize diffusion dominated transport of analytes, which is limited by slow reaction rates and long detection times. By integrating alternating current (AC) electrokinetics and electrochemical impedance spectroscopy (EIS), we construct an immunochip for rapid, sensitive, and label-free detection. AC electroosmosis (ACEO) and positive dielectrophoresis (DEP), induced by a biased AC electric field, can rapidly convect and trap the analyte onto an EIS working electrode within a few minutes. This allows the change of electron-transfer resistance (ΔR_{et}) caused by the antibody–antigen (IgG–protein A) binding to be measured and quantified in real time. The measured impedance change achieves a plateau after electrokinetic concentration for only 90 s, and the detection limit is able to reach 200 pg ml^{-1}. Compared to the conventional incubation method, the electrokinetics-enhanced method is approximately 100 times faster in its reaction time, and the detection limit is reduced by 30 times. The ΔR_{et} of the positive response is two orders of magnitude higher than the negative control, demonstrating excellent specificity for practical applications.

1 Introduction

In recent years, immunoassays have become powerful and versatile biomedical tools for the diagnosis of certain food toxins, environmental pollutants, or clinical diseases.[1,2] Because of the specific binding between antibodies and antigens, immunoassays have been widely used to selectively bind biomolecules known as biomarkers that are indicative of the presence of bacteria, viruses, or proteins.[3–6] Conventional immunoassays such as the enzyme-linked immuno-sorbent assay (ELISA) and the Western blot are typically limited by their portability and are of high cost because they need elaborate fluorescent/enzyme tagging and sophisticated optical instruments.[2,7] Label-free detection is necessary for in-field diagnoses that can avoid large and expensive optical systems by reducing the size of the required equipment. Recently, label-free detection methods using techniques such as electrochemical impedance spectroscopy (EIS),[8] surface plasmon resonance (SPR),[9] quartz crystal microbalance (QCM),[10] surface enhanced Raman spectroscopy (SERS),[11] nanowire-based and cantilever-based biosensors[12,13] have been developed to study the characteristics of surface modifications, antibody–antigen binding and DNA–DNA hybridization without fluorescent labelling/tagging. In recent years, electrochemical based immuno-biosensors have been widely utilized to detect specific proteins and bacteria.[14,15] Not only because they have the advantages of convenience, miniaturization, and low cost, but they also do not require sophisticated equipment.[7,16–18] However, commonly used surface-based detection platforms rely on surface-bound reactions. These reactions, under low analyte concentrations, rely on the diffusion-dominated transporting kinetics to move the target molecules/proteins to the detection surface. This mechanism is quite slow and reactions may not even occur, resulting in the limitations of low sensitivity and long reaction time (3–4 h).[19,20] As a result, there is a need to develop a rapid, label-free, and highly sensitive detection platform for rapid screening and field-use applications ranging from proteomics to pathogen identification.[21,22] Several methods, such as hydrodynamic, acoustic, and electrokinetic mixing, have been employed to increase the reaction rate of antibody–antigen binding.[23–25] In the past few years, electrokinetics has been used to manipulate analytes. For example, target DNA has been moved to probe-immobilized surfaces successfully using direct current (DC) electric fields.[26,27] AC electroosmosis (ACEO) has been proposed and used in pumping liquids and concentrating microbes and DNA molecules;[28–31] dielectrophoresis (DEP) has also been utilized in the separation and concentration of targets

[a]National Nano Device Laboratories, National Applied Research Laboratories, Tainan, Taiwan, ROC

[b]Department of Biomedical Engineering, National Cheng Kung University, Tainan, 701, Taiwan, ROC. E-mail: hcchang@mail.ncku.edu.tw

[c]Institute of Nanotechnology and Microsystems Engineering, National Cheng Kung University, Taiwan

[d]Center for Micro/Nano Science and Technology, National Cheng Kung University, Taiwan

[e]Medical Device Innovation Center, National Cheng Kung University, Taiwan

† Electronic supplementary information (ESI) available. See DOI: 10.1039/c3an00190c

being analysed.[20,32–34] Dielectrophoretic manipulation of proteins and small molecules has also been presented,[35,36] and DEP-based microfluidic devices for the detection of molecular binding events have been presented.[37,38] However, small electrode dimensions or a high applied voltage is required to generate sufficiently high DEP forces to manipulate small molecules effectively ($F_{DEP} \sim r^3 \nabla E^2$).

In this research, biased ACEO was employed to transport biomolecules by fluid convection to an antibody-immobilized electrode, and AC DEP was also used to rapidly trap the concentrated molecules at the surface of an antibody-immobilized electrode. Using these electrokinetic tools, the affinity binding could be accelerated, thus significantly enhancing the sensitivity, binding efficiency, and reaction rate. After the electrokinetic concentration, a label-free EIS method was used to detect and quantify the antibody–antigen binding in real time. Because of the electrokinetic enhancement, the sensitivity could be enhanced by at least one order of magnitude (compared to the ELISA kit) to reach a sub-ng ml^{-1} level, and the detection time could be reduced from several hours to a few minutes. To our knowledge, enhanced analyte binding using AC electrokinetics combined with detection using EIS on an immuno-chip has not been reported in the literature. The specificity, sensitivity, and frequency-dependent reaction rates are also investigated in this article to address the practical applications of this novel method.

2 Materials and methods

2.1 Theory and design

AC electroosmosis is caused by the interaction between a non-uniform AC electric field and the electric double layer that is induced *via* accumulating charges near the surface of the polarized electrode. Electric field-induced ion migrations drag the fluid to generate a bulk flow over the electrodes. Therefore, the diffusion-limited barrier in the antibody–antigen binding can be overcome by the ACEO-induced fluid motion and positive DEP attraction. The flow velocity of ACEO that is induced by the AC electric field can be described as follows:[39]

$$v_{ACEO} = \frac{\varepsilon {V_0}^2 \Omega^2}{8\eta x\left(1+\Omega^2\right)^2} \quad \Omega = \omega \frac{\varepsilon}{\sigma}\frac{\pi}{2}x\kappa \tag{1}$$

where σ and ε are the conductivity and permittivity of the medium, respectively; x is the characteristic length of the electrode separation; η is the viscosity of the fluid; V_0 is the applied AC voltage; Ω is the non-dimensional frequency; and k^{-1} (Debye length) is the thickness of the electric double layer (EDL), which can be described by the following formula:

$$\frac{1}{\kappa} = \lambda_D = \sqrt{\frac{\varepsilon_m kT}{2F^2 Z^2 C_i}}. \tag{2}$$

The characteristic frequency of ACEO can be approximated as the inverse resistance–capacitance (R–C) charge relaxation time and is related to k^{-1}, σ, and ε. It can be described as follows:

$$\omega_0 \sim (RC)^{-1} = \sigma/(C_{DL}x). \tag{3}$$

As shown by the above formulae, the characteristic frequency of the ACEO shifts with changes in conductivity, electrode gaps, and the thickness of the EDL. According to eqn (1) and (2), the velocity of the ACEO decreases with increasing conductivity of the solution because of the fact that a high ionic strength would make the EDL thinner. Therefore, the appropriate conductivity for sufficient ACEO generation is in the range between 1 and 10 mS m^{-1}.[28] Biased ACEO combines a DC bias with AC signals to generate two electrode charging effects, capacitive charging and Faradaic charging on different electrodes. This asymmetric polarization is capable of inducing fluid convection more effectively and could be used in a wider range of buffer conductivities to induce sufficiently high convections.[29,40,41]

AC DEP is the electric-field-induced motion of objects by dielectric polarization. The dielectrophoretic force is defined by $F_{DEP} = 2\pi r^3 \varepsilon_m \mathrm{Re}[f_{CM}(\omega)]\nabla E^2$. E is the applied electric field, r is the radius of the particle and $\mathrm{Re}(f_{CM})$ is the real part of the Clausius–Mossotti (CM) factor. If particles are more polarizable than the surrounding medium, they will be attracted to the relatively strong region of the electrical field gradient ($\mathrm{Re}[f_{CM}(\omega)] > 0$, positive DEP); if particles are less polarizable than the surrounding medium, they will be repelled to the relatively weak region of the electrical field gradient ($\mathrm{Re}[f_{CM}(\omega)] < 0$, negative DEP).

Our chip has a concentric electrode design consisting of two platinum (Pt) electrodes and one gold (Au) electrode for the electrochemical counter, reference and working electrodes, respectively, and thus could simultaneously be used for the electrokinetic concentration and the EIS measurement, as shown in Fig. 1(a). In this research, biased electroosmosis (ACEO) is utilized to generate vortexes to transport and concentrate the suspended proteins into a stagnation area on the EIS working electrode, and the proteins were accelerated to contact the immunoglobulin G (IgG)-modified surface by the positive dielectrophoretic force (Fig. 1(b)).

2.2 Experimental setup

Detecting antibody–antigen interactions using electrochemical impedance spectroscopy (EIS) by measuring the changes in impedance between antibody–antigen binding and non-binding is feasible. The system configuration is shown in Fig. 1. An AC voltage with a DC bias was applied to generate electrokinetic forces to concentrate and trap proteins/particles using a function generator (WAVETEK 195). The electrokinetic behavior of particles was observed using an inverted microscope (CH 40, Olympus) with a fluorescent light source, and the results were recorded using a high speed CCD camera (20 frames per second, Microfire, OPTRONICS). By connecting to an impedance analyzer (IM6, Zahner Company), the micro-fabricated counter, reference, and working electrodes were used to measure the impedance changes caused by antibody–antigen interactions using a frequency ranging from 100 Hz to 100 kHz. The measured impedance spectrum was analyzed using the THALES analysis software. The electron-transfer resistance R_{et}

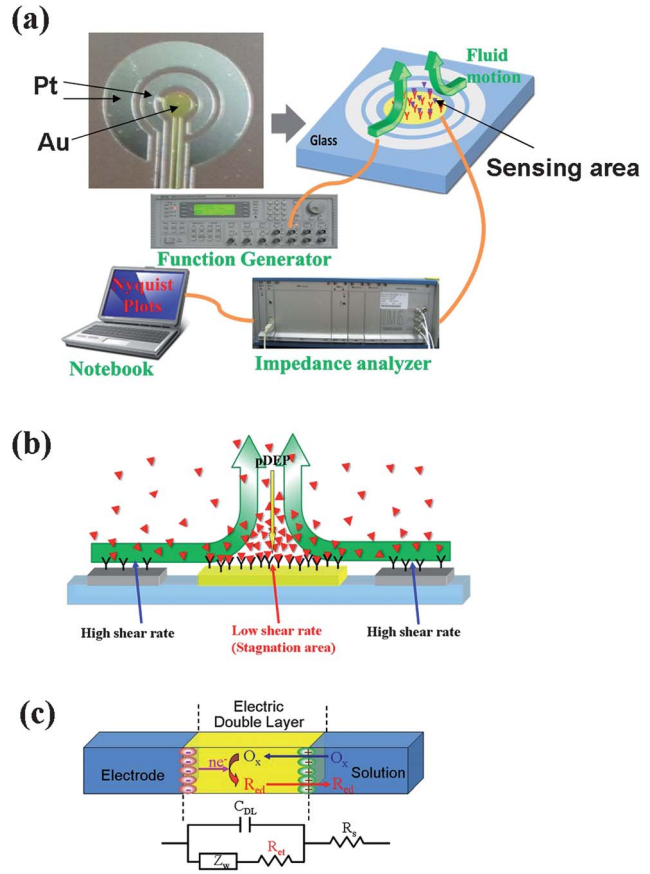

Fig. 1 (a) Configuration of the experimental setup. A function generator supplied an AC voltage to induce AC electrokinetic forces to concentrate proteins onto an antibody-immobilized Au electrode, and the antibody–antigen binding was then measured using an impedance analyzer for the quantification of the analyte. (b) Schematic illustration of ACEO convection and positive DEP trapping. (c) The measured EIS data were simulated with an equivalent circuit to analyze the impedance changes in ΔR_{et}.

could be estimated by fitting the impedance data based on a simulated equivalent circuit mode (Randles model), as shown in Fig. 1(c).

2.3 Microchip fabrication

The detection chip consisted of a circular Au electrode in the centre as an EIS working electrode (200 μm in diameter) and two Pt ring-shaped electrodes. The inner Pt electrode serves as the reference electrode with a width of 100 μm and an outer electrode as the counter electrode with a width of 200 μm. To fabricate two types of metal surfaces for on-chip EIS measurements and for selective modification, two photolithographic processes were used. First, the positive photoresist (Shipley 1818) was spin-coated on an Au/Ti (titanium) deposited glass slide (Kimble, 76 × 26 × 1 mm thick). The electrode geometry was determined through standard photolithography, and then metal etching was used to pattern the Au working electrode. Counter and reference electrodes were fabricated using a lift-off process. A reversible photoresist, AZ 5214E (MicroChem Corp., USA), was spin-coated on the Au-patterned slide. Image reversal photolithography was subsequently used to produce the reverse pattern, and then 100 nm/20 nm thick Pt/Ti layers were deposited on the patterned slides using RF-sputtering. The electrode geometries were determined after removing the photoresist using acetone. The flow chart for the fabrication processes is shown in Fig. 2. The concentric-circle electrodes were fabricated on a glass substrate with two different metals (Au and Pt); the two metals were used not only to transport (by ACEO) and trap (by DEP) molecules on the antibody-modified electrode, but they could also be used for selective chemical modifications and for the purpose of EIS measurements. The fact that the binding energy of Pt is much lower than that of Au allows the selective chemical modifications.[42]

2.4 Electrode modification

A piranha solution (H_2O_2 : H_2SO_4 = 3 : 7) was used to clean the surface of the fabricated microelectrodes before surface modifications. The piranha-cleaned electrodes were immersed in an 11-MUA solution (5 mM in absolute ethanol) for 30 min at room temperature to form a sulphide-based SAM (self-assembled monolayer). 1-Ethyl-3-(3-dimethylaminopropyl) carbodiimide (EDC) and *N*-hydroxysuccinimide (NHS) were subsequently dissolved in an MES buffer (2-(*N*-morpholino) ethanesulfonic acid, 50 mM, pH = 5.5), and the mixture was used to activate the COOH group on the Au-SAM surface. The mouse IgG antibody was incubated on the electrodes with stable shaking for 1 h, and the surface was washed with phosphate buffer solution (PBS) three times. After IgG immobilization, 1% BSA was used to block the non-IgG immobilized areas.

Cyclic voltammetry (CV) was used to build a better understanding of the electron-transfer rate on the modified electrodes. The oxidation and reduction peaks could be observed clearly at approximately −0.08 V and 0.04 V for the microfabricated bare Au electrode (Fig. S1(a)†). The immobilization of IgG and BSA on the 11-MUA-coated electrode resulted in a descending current response. A detailed description is provided in the ESI.†

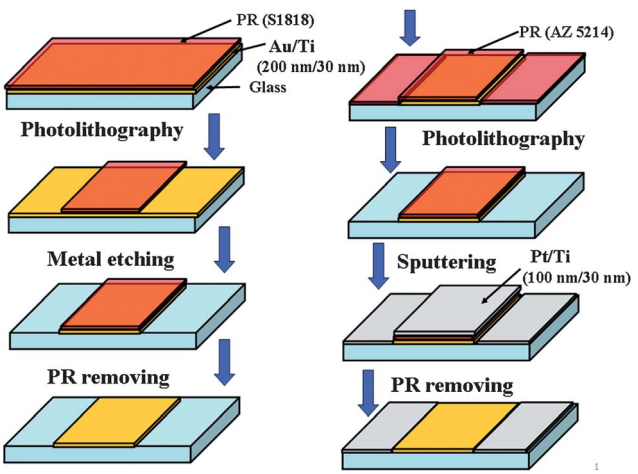

Fig. 2 Fabrication processes for microelectrodes containing the Pt reference and counter electrodes and an Au working electrode.

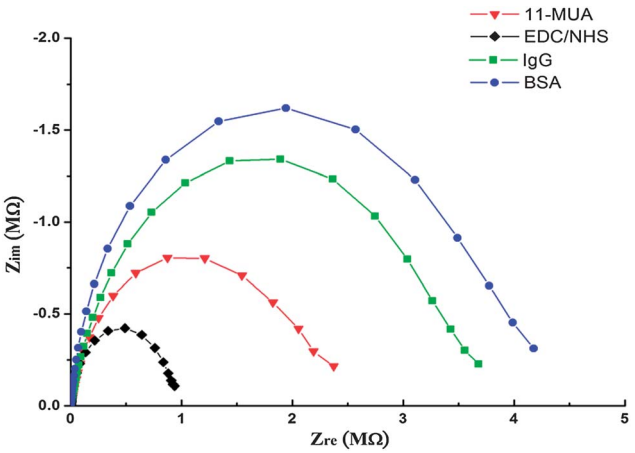

Fig. 3 Nyquist plots of different modification layers, a bare Au, 11-MUA/Au, EDC-NHS/11-MUA/Au, IgG/EDC-NHS/11-MUA/Au, BSA/IgG/EDC-NHS/11-MUA and protein A/BSA/IgG/EDC-NHS/11-MUA/Au electrodes, respectively.

The electron-transfer resistance R_{et} caused by different modification layers was fitted by a Randles circuit model (Fig. 1(c)). The supporting solution for EIS measurements is an MES (20 mM, pH = 5) solution containing $[Fe(CN)_6]^{3-/4-}$ (2.5 mM, 1 : 1) with 100 mM KCl. The applied frequency ranges from 0.1 Hz to 100 kHz (AC: 5 mV, DC: −0.02 V *vs.* Pt). After the 11-MUA modification, the diameter of the half-circle of the Nyquist plot clearly increased, and the Warburg impedance disappeared, as shown in Fig. 3. The progressive addition of 11-MUA, BSA and IgG contributed to the insulation properties of the surface to obstruct electron transfer to the Au surface; thus, the electron-transfer resistance R_{et} increased when the Au surface was modified stepwise, as shown in Fig. 3. Moreover, the R_{et} component for individual modification layers appears to have evident differences, which is indicative of high sensitivity in the microelectrode-based EIS detection.

3 Results and discussion

3.1 Optimal frequency of ACEO concentration for EIS detection

The optimal detecting conditions should be frequency dependent because ACEO and DEP are very sensitive to the applied frequency of the AC voltage and the ionic strength of a solution (eqn (1) and (2)).

Fluorescent latex beads (d = 20 nm, concentration ~1.2×10^8 ml^{-1}) suspended in 0.01 × PBS buffer ($\sigma \sim 150$ μS cm^{-1}) were used to test and observe the characteristics of electrokinetic concentration at various applied frequencies, and to identify the optimal frequency to effectively concentrate the analytes on the EIS working electrode. The previous study has mentioned that the nano-scale particles exhibit positive DEP at low frequency, and its cross-over frequency is with respect to the product of the Debye length and the particle size.[43] The upper boundary of the positive DEP frequency window corresponds to the inverse polarization time of the molecule. Earlier experiments on small molecules and nanocolloids[44,45] show that there is a frequency window (at low frequency) in which the molecule exhibits positive DEP. A DC voltage of 0.5 V was biased to AC voltages of '15 V_{pp}', '8 V_{pp}' and the ground that were sustained on the outer ring-shaped, the inner ring-shaped and the central circular-shaped electrodes, respectively. This strategy induced strong Faradaic charging and capacitive charging simultaneously, which enabled the targets to be transported toward the central electrode. We suppose that the DEP force induced by the field strength of 10^5 V m^{-1} should be very weak and can be ignored when the particle size is smaller than tens of micrometers. Therefore, the effective DEP force could only occur near the stagnation area. Various frequencies were used to induce AC electrokinetic forces (biased ACEO and DEP) to accumulate fluorescent nanobeads in the desired area for measurements (Fig. 4(a)). Fig. 4(a) shows the results of the concentrated fluorescent nanobeads at different applied frequencies. The image data were obtained by applying an AC electric field for 60 s. Fig. 4(a1 and a2) show that nanobeads were condensed at the centre electrode with a wide area distribution. This could be attributed to the interaction of a lower ACEO coupled with a strong DEP force in the stagnation area, and therefore, the particles cannot be transported to and concentrated at a small region. The optimal frequencies for concentrating molecules for optical detection were identified as 2 and 3 kHz, as shown in Fig. 4(a3 and a4). When the alternating frequency is faster than the inverse of the charge relaxation time (>10 kHz) required for the capacitive charging, the ACEO effect became negligible and the particles could not be transported into the centre region by a negligible ACEO flow. The magnitude of the induced electrothermal flow is approximately two orders lower than ACEO at low frequency when the buffer conductivity is tens of mS m^{-1}.[46] Therefore, in our study, the effect of electrothermal flow may be neglected.

An ideal situation for electrokinetic concentration is the promotion of EIS detection, which is capable of concentrating a high number of proteins/molecules distributed on an antibody-immobilized electrode in order to achieve a high impedance response. In this study, the electron-transfer impedance of a modified electrode was investigated for the purpose of analyzing the antibody–antigen binding. The target protein A was suspended in 0.01× PBS buffer ($\sigma \sim 150$ μS cm^{-1}). An AC voltage with a DC bias was applied to induce the biased ACEO for concentration of analytes. After ACEO concentration, the applied signal was switched off, the analytes were subsequently washed three times with PBS buffer, and the buffer was changed to an MES (20 mM, pH = 5) solution containing $[Fe(CN)_6]^{3-/4-}$ (2.5 mM, 1 : 1) with 100 mM KCl for EIS measurements. For EIS measurement, the applied frequency ranges from 0.1 Hz to 100 kHz (AC: 5 mV, DC: −0.02 V *vs.* Pt) from an impedance analyzer. To investigate the frequency-dependent impedance change after the electrokinetic concentration, various frequencies of 0.5, 0.8, 0.9, 1, and 3 kHz were applied with a protein concentration of 20 ng ml^{-1}. Fig. 4(b) shows the magnitudes of the increased impedance after an electrokinetic concentration for 30 s by applying various frequencies. The maximum impedance change of approximately 22 MΩ occurred at a frequency of 800 kHz. Here, ACEO plays a role in transporting the protein molecules

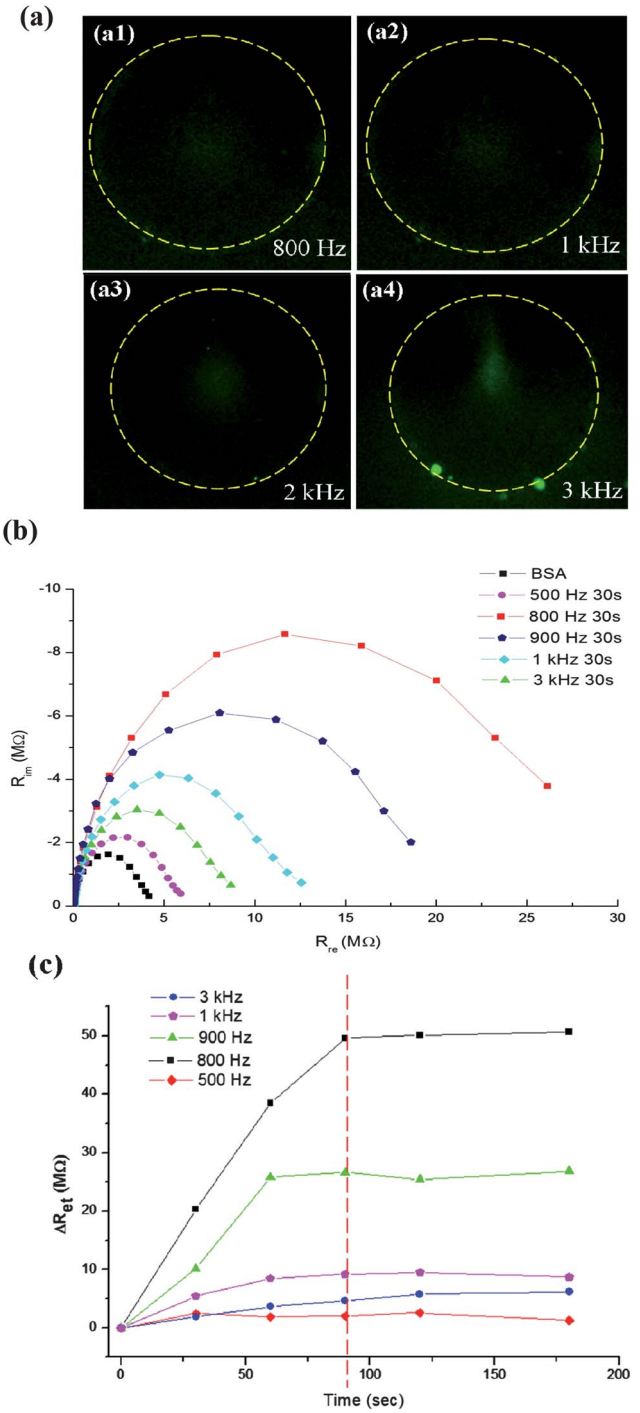

Fig. 4 (a) Images of electrokinetic concentration of 20 nm particles after applying an AC voltage at a frequency of (a1) 800 Hz, (a2) 1 kHz, (a3) 2 kHz and (a4) 3 kHz for 60 s, respectively. (b) Experimental results of EIS-measured impedance changes after electrokinetic concentration at different frequencies. (c) The plateau time for the impedance increases at different applied frequencies induced electrokinetic concentrations.

toward the centre electrode; moreover, the electrokinetics (DEP and EP) assist them in rapidly attaching to the immobilized IgG. This result could be attributed to the fact that, under these conditions, an appropriate strength of the biased ACEO convection is capable of transporting the proteins into the central electrode region, and positive DEP also provides a sufficiently high attraction force to trap the transported proteins in the area of the centre electrode. An optimal concentrating condition for EIS measurement occurred at a frequency of 800 Hz, at which the largest number of analytes attached to the surface of the EIS working electrode, thus resulting in the largest impedance change.

In the frequency range from 1 kHz to 3 kHz, the violent biased ACEO substantially overcame the molecular dielectrophoretic and electrophoretic forces, and thus, the concentrated molecules could overlap in a small stagnation area. This scenario reduced the number of antibody–antigen bindings on the EIS working electrode surface, which resulted in a lower ΔR_{et}, as shown in Fig. 4(b). Therefore, trapping small molecules on the electrode surface as shown in the pattern of Fig. 4(a1 and a2) could be better for EIS detection and could only occur in a narrow band of frequencies, 800–1000 Hz (Fig. 4(c)). Nevertheless, the highest impedance change ΔR_{et} for molecules occurred at 800 kHz. These results are also in agreement with our predictions from the results of fluorescence observation in Fig. 4(a). When the frequency was higher than 5 kHz, the analytes could not be transported to the EIS working electrode effectively due to the weak ACEO and short-range DEP effect, thus also resulting in a lower ΔR_{et}. The optimal frequency for trapping 20 nm beads and protein molecules could be different due to the influence of the surface charge- and size-dependent DEP force.

3.2 Impedance increase to reach a plateau *versus* different applied frequencies

To study the time for the impedance increase to reach a plateau (plateau time), the predetermined driving voltage was applied for 0, 30, 60, 90, 120 and 180 s at different frequencies (500 Hz, 800 Hz, 900 Hz, 1 kHz and 3 kHz, respectively). Fig. 4(c) shows ΔR_{et} as a function of the electrokinetic reaction time at a protein concentration of 20 ng ml^{-1}. An optimal frequency of 800 Hz was found, and its impedance change reached a plateau ($\Delta R_{et} \sim 50$ MΩ) after an AC electrokinetic concentration for only 90 s. All the other electrokinetics-assisted bindings at other frequencies also reached plateaus within 90 s, but the saturated ΔR_{et} values were much lower than the optimal one. The results indicated that the optimal concentrating time to detect affinity responses by EIS at an optimal frequency of 800 Hz would be 90 s, and these conditions were also used to further investigate the detection limit.

The plateau time as a function of different protein concentrations was also studied to investigate the shortest reaction time for the subsequent EIS measurements. EIS data were obtained after electrokinetic concentrations for 30, 60, 90, and 120 s. Table S1† (in the ESI) shows the results for the plateau time of ΔR_{et} at different protein concentrations. The molecules could continuously be accumulated on the micro-fabricated EIS working electrode, and the plateau time at protein concentrations of 20 ng ml^{-1}, 2 ng ml^{-1} and 0.2 ng ml^{-1} was found to be 90 s, 60 s and 30 s, respectively. The tendency of the results shows that the plateau time is shorter with lower protein

concentrations. Therefore, 90 s was used to concentrate proteins with various concentrations in the rest of the experiments to achieve a plateau.

3.3 Specificity and detection limit

The non-specific binding with heterogeneous samples can cause false positive results; therefore, ELISA and Western blot kits generally use several repeated wash steps to reduce non-specific bindings. These wash steps can also reduce the reported signal, thus decreasing the sensitivity and causing false negative results at low target concentrations. To examine the specificity of our platform, another protein, avidin at a concentration of 20 ng ml^{-1}, was used as a negative control. The measured ΔR_{et} was only 0.4 MΩ after ACEO concentration of avidin for 90 s, as shown in Fig. 5(a and a1). Compared to the positive response (protein A), which reached approximately 50 MΩ, the difference in the ΔR_{et} obtained was two orders of magnitude higher, demonstrating excellent specificity (Fig. 5(a)). ΔR_{et} also reached approximately 2.4 MΩ when the antigen concentration was as low as 0.2 ng ml^{-1} (Fig. 5(a and b)). It is discriminable, and the *S*/*N* ratio is higher than five compared to the negative control. The result of high specificity could be attributed to the low ionic strength buffer that we used. The lower ionic strength could provide a stronger electrostatic repulsion force on the molecular surface (Cheng *et al.* 2012), resulting in a reduction in non-specific binding (see the details in Fig. S2 in the ESI†).

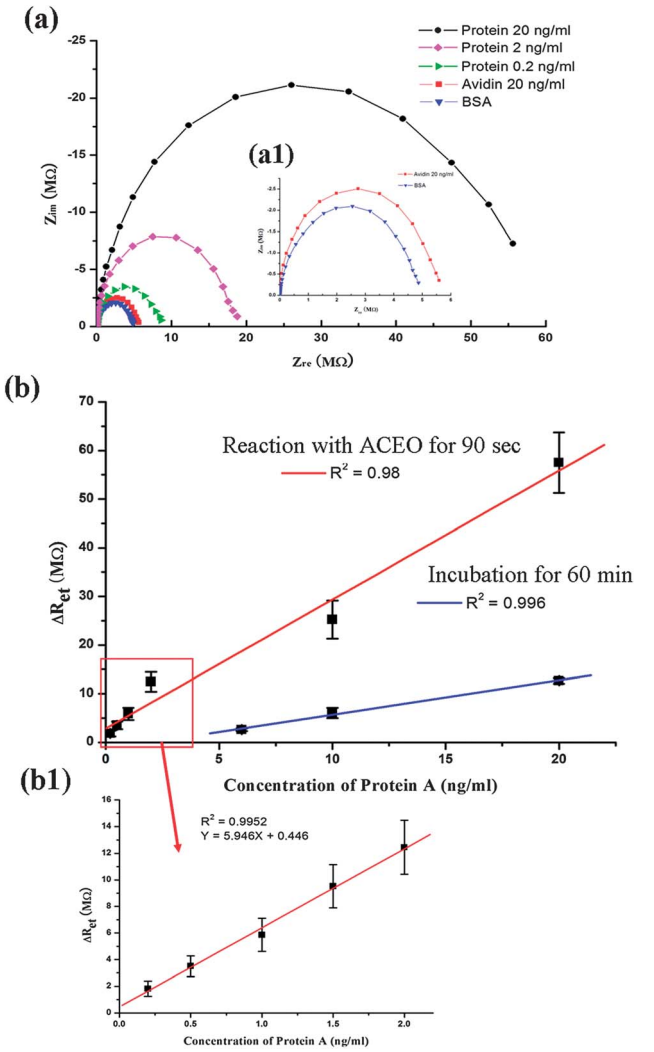

Fig. 5 (a) Nyquist plots of a positive response (protein A) and the negative control (avidin). The positive response of protein A reached 57 MΩ, and (a1) the negative control was only 0.47 MΩ, which demonstrated excellent specificity. (b) ΔR_{et} with/without electrokinetic concentration *versus* different protein concentrations. The impedance was measured after electrokinetic concentration of protein A for 90 s. The detection limit of the electrokinetics-enhanced reaction reached 0.2 ng ml^{-1}, and the reaction time was reduced from 1 h to 90 s. (b1) The R^2 value in the range between 0.2 and 2 ng ml^{-1} reached 0.9949.

To investigate the linearity of the quantification and detection limit, different protein concentrations from 0.2 to 20 ng ml^{-1} were used. The antibody–antigen binding was enhanced electrokinetically for 90 s and the impedance change (ΔR_{et}) caused by the binding was measured using EIS. Fig. 5(b) shows that ΔR_{et} increases as a function of increasing concentrations of protein (data are averaged over five runs with different chips). The results show that the detection limit reached 0.2 ng ml^{-1} (approximately 1–2 orders of magnitude lower than the conventional ELISA kit), and the R^2 value between 0.2 ng ml^{-1} and 20 ng ml^{-1} reached 0.9818. Additionally, the R^2 value in the range between 0.2 and 2 ng ml^{-1} reached 0.9949 (Fig. 5(b1)). At high analyte concentrations, a large number of analytes is transported to the central electrode surface where the concentrated analytes could overlap, and therefore the slope of impedance changes could tend to be gradual. However, the two linear correlation regions of 0.2–2 ng ml^{-1} and 2–20 ng ml^{-1} could be used to separately quantify the analytes by using the two different correlation coefficients. Based on the above results, this good linearity indicated the possibility to quantify the target of interest. The electrokinetics-enhanced method was also compared with the conventional incubation method to study the enhancement. For the incubation method on our chip, the IgG–protein A binding occurred for 1 h in a PBS solution at room temperature. The detection limit of the electrokinetics-enhanced method (0.2 ng ml^{-1}) was 30 times higher than that of the incubation method (6 ng ml^{-1}), as shown in Fig. 5(b), and the reaction rate was significantly accelerated from 1 h to 90 s. In high ionic strength fluids, the dominant electrohydrodynamics changes to AC electrothermal flow, and its working frequencies would shift to higher frequencies (above 100 kHz). This could be a good future research topic in AC electrokinetics-enhanced biosensors.

4 Conclusions

A label-free, rapid, and highly sensitive (sub-nM sensitivity) immunoassay that combines ACEO concentration, DEP attraction, and EIS detection has been proposed, designed and demonstrated. The changes in the impedance spectrum were measured after AC electrokinetic concentration (at an optimal frequency of 800 Hz) for 90 s. ΔR_{et} reached as high as 57 MΩ and 2.38 MΩ for protein concentrations of 20 ng ml^{-1} and 0.2 ng ml^{-1}, respectively. The reaction rate was enhanced by coupling electric

field-induced vortices and electrokinetics (electrophoresis and pDEP). Compared to the conventional incubation method, the detection time was thus reduced 100 times (~90 s); furthermore, the detection limit reached 200 pg ml^{-1} (30 times lower than the conventional incubation method). Finally, the impedance change from the positive response (protein A) was two orders of magnitude higher than the negative control (avidin), which provided excellent specificity. This rapid and label-free platform may be further used in the detection of DNA hybridizations and viral infections and has the potential to be developed into a field-use assay.

Acknowledgements

This study was supported by research grants from the National Science Council (and NSC 100-2221-E-006-026-MY3 and NSC 101-2218-E-492-002-), the Medical Device Innovation Center, National Cheng Kung University, the Multidisciplinary Center of Excellence for Clinical Trial and Research (DOH102-TD-B-111-002), and the Department of Health, Executive Yuan, Taiwan. We also thank the National Nano Device Laboratory for supplying the micro-fabrication equipment.

References

1 D. S. Hage, *Anal. Chem.*, 1995, **67**, 455–462.
2 R. M. Lequin, *Clin. Chem.*, 2005, **51**, 2415–2418.
3 D. S. Hage, *Anal. Chem.*, 1993, **65**, 420–424.
4 A. K. Deisingh and M. Thompson, *Analyst*, 2002, **127**, 567–581.
5 C. A. K. Borrebaeck, *Immunol. Today*, 2000, **21**, 379–382.
6 K. Jasbeer, F. M. Ghazali, Y. K. Cheah and R. Son, *ASEAN Food J.*, 2008, **15**, 1–25.
7 C.-S. Chen, K.-N. Chang, Y.-H. Chen, C.-K. Lee, B. Y.-J. Lee and A. S.-Y. Lee, *Biosens. Bioelectron.*, 2011, **26**, 3072–3076.
8 A.-E. Radi, X. Muñoz-Berbel, V. Lates and J.-L. Marty, *Biosens. Bioelectron.*, 2009, **24**, 1888–1892.
9 E. A. Perkins and D. J. Squirrell, *Biosens. Bioelectron.*, 2000, **14**, 853–859.
10 Y.-C. Liu, C.-M. Wang, K.-P. Hsiung and C. Huang, *Biosens. Bioelectron.*, 2003, **18**, 937–942.
11 C. Song, Z. Wang, R. Zhang, J. Yang, X. Tan and Y. Cui, *Chin. Opt. Lett.*, 2010, **8**, 309–312.
12 W. U. Wang, C. Chen, K.-H. Lin, Y. Fang and C. M. Lieber, *Proc. Natl. Acad. Sci. U. S. A.*, 2005, **102**, 3208–3212.
13 G. H. Wu, R. H. Datar, K. M. Hansen, T. Thundat, R. J. Cote and A. Majumdar, *Nat. Biotechnol.*, 2001, **19**, 856–860.
14 M. S. Chiriac, E. Primiceri, E. D'Amone, R. E. Ionescu, R. Rinaldiac and G. Maruccio, *Lab Chip*, 2011, **11**, 658–663.
15 M. Sen, K. Ino, H. Shiku and T. Matsue, *Lab Chip*, 2012, **12**, 4328–4335.
16 T. G. Drummond, M. G. Hill and J. K. Barton, *Nat. Biotechnol.*, 2003, **21**, 1192–1199.
17 J. Wu, J. Tang, Z. Dai, F. Yan, H. Ju and N. E. Murr, *Biosens. Bioelectron.*, 2006, **22**, 102–108.
18 H. Qi, C. Wang and N. Cheng, *Microchim. Acta*, 2010, **170**, 33–38.
19 K. Kerman, M. Vestergaard and E. Tamiya, *Methods Mol. Biol.*, 2009, **504**, 99–113.
20 I.-F. Cheng, S. Senapati, X. Cheng, S. Basuray, H.-C. Chang and H.-C. Chang, *Lab Chip*, 2010, **10**, 828–831.
21 S. Choi, M. Goryll, L. Y. M. Sin, P. K. Wong and J. Chae, *Microfluid. Nanofluid.*, 2011, **10**, 231–247.
22 X. Weng, H. Jiang and D. Li, *Microfluid. Nanofluid.*, 2011, **11**, 367–383.
23 K.-Y. Lien, J.-L. Lin, C.-Y. Liu, H.-Y. Lei and G.-B. Lee, *Lab Chip*, 2007, **7**, 868–875.
24 F. Kardous, A. Rouleau, B. Simon, R. Yahiaoui, J. F. Manceau and W. Boireau, *Biosens. Bioelectron.*, 2010, **26**, 1666–1671.
25 N. Sasaki, T. Kitamori and H.-B. Kim, *Lab Chip*, 2006, **6**, 550–554.
26 C. F. Edman, D. E. Raymond, D. J. Wu, E. Tu, R. G. Sosnowski, W. F. Bulter, M. Nerenberg and M. J. Heller, *Nucleic Acids Res.*, 1997, **25**, 4907–4914.
27 J. Cheng, E. L. Sheldon, L. Wu, A. Uribe, L. O. Gerrue, J. Carrino, M. J. Heller and J. P. O. 'Connell, *Nat. Biotechnol.*, 1998, **16**, 541–546.
28 P. K. Wong, C.-Y. Chen, T.-H. Wang and C.-M. Ho, *Anal. Chem.*, 2004, **76**, 6908–6914.
29 J. Wu, Y. Ben and H.-C. Chang, *Microfluid. Nanofluid.*, 2005, **1**, 161–167.
30 M. R. Brown and C. D. Meinhart, *Microfluid. Nanofluid.*, 2006, **2**, 513–523.
31 R. Hart, R. H. Lec and M. Noh, *Sens. Actuators, B*, 2010, **147**, 366–375.
32 C. Tlili, L. N. Cella, N. V. Myung, V. Shetty and A. Mulchandani, *Analyst*, 2010, **135**, 2367–2642.
33 I.-F. Cheng, C.-C. Lin, D.-Y. Lin and H.-C. Chang, *Biomicrofluidics*, 2010, **4**, 034104.
34 K. Khoshmanesh, S. Nahavandi, S. Baratchi, A. Mitchell and K. Kalantar-zadeh, *Biosens. Bioelectron.*, 2011, **26**, 1800–1814.
35 B. H. Lapizco-Encinas, S. Ozuna-Chaco'n and M. Rito-Palomares, *J. Chromatogr., A*, 2008, **1206**, 45–51.
36 A. Nakano, F. Camacho-Alanis, T.-C. Chao and A. Ros, *Biomicrofluidics*, 2012, **6**, 34108.
37 M. Viefhues, J. Regtmeier and D. Anselmetti, *Analyst*, 2013, **138**, 186–196.
38 I.-F. Cheng, H.-W. Han and H.-C. Chang, *Biosens. Bioelectron.*, 2012, **33**, 36–43.
39 N. G. Green, A. Ramos, A. González, H. Morgan and A. Castellanos, *Phys. Rev. E: Stat. Phys., Plasmas, Fluids, Relat. Interdiscip. Top.*, 2000, **61**, 4011–4018.
40 J. Wu, *IEEE Transactions on Nanotechnology*, 2006, **5**, 84–89.
41 M. Lian and J. Wu, *Appl. Phys. Lett.*, 2009, **94**, 064101.
42 A. Steude, S. Schmidt, A. A. Robitzki and O. Panke, *Lab Chip*, 2011, **11**, 2884–2892.
43 S. Basuray and H.-C. Chang, *Phys. Rev. E: Stat., Nonlinear, Soft Matter Phys.*, 2007, **75**, 060501.
44 C. L. Asbury, A. H. Diercks and G. V. D. Engh, *Electrophoresis*, 2002, **23**, 2658–2666.
45 H. Morgan, M. P. Hughes and N. G. Green, *Biophys. J.*, 1999, **77**, 516–525.
46 D. F. Chen and H. Du, *J. Micromech. Microeng.*, 2006, **16**, 2411–2419.